SCIENTIFIC REPORTS

OPEN

SUBJECT AREAS:
BIOPHYSICS
ANTIMICROBIALS
BIOCHEMISTRY
ANTIFUNGAL AGENTS

Received
23 July 2012

Accepted
18 September 2012

Published
29 October 2012

Correspondence and requests for materials should be addressed to D.B. (dave.barlow@kcl.ac.uk)

Neutron diffraction studies of the interaction between amphotericin B and lipid-sterol model membranes

Fabrizia Foglia[1], M. Jayne Lawrence[1], Bruno Demé[2], Giovanna Fragneto[2] & David Barlow[1]

[1]Institute of Pharmaceutical Science, King's College London, London, UK, [2]Institut de Laue Langevin, Grenoble, France.

Over the last 50 years or so, amphotericin has been widely employed in treating life-threatening systemic fungal infections. Its usefulness in the clinic, however, has always been circumscribed by its dose-limiting side-effects, and it is also now compromised by an increasing incidence of pathogen resistance. Combating these problems through development of new anti-fungal agents requires detailed knowledge of the drug's molecular mechanism, but unfortunately this is far from clear. Neutron diffraction studies of the drug's incorporation within lipid-sterol membranes have here been performed to shed light on this problem. The drug is shown to disturb the structures of both fungal and mammalian membranes, and co-localises with the membrane sterols in a manner consistent with trans-membrane pore formation. The differences seen in the membrane lipid ordering and in the distributions of the drug-ergosterol and drug-cholesterol complexes within the membranes are consistent with the drug's selectivity for fungal *vs.* human cells.

Recent years have witnessed a dramatic rise in the frequency of invasive fungal infections – which has led to significant increases in morbidity and mortality in immuno-compromised patients[1–3] - and also to an increased resistance of the pathogenic fungi to therapy[4–6] – including resistance to one of the mainstays of the anti-mycotic armoury, amphotericin B (AmB)[7–9]. The usefulness of AmB, moreover, has always been limited by its narrow therapeutic index[10], and the recent use of elevated levels to treat resistant fungal infections – with complications arising due to the ensuing renal insufficiency - has frequently proved unsuccessful[11]. Combating these problems through the development of new anti-mycotics requires a detailed knowledge of the molecular mechanism of AmB, but unfortunately this is far from fully understood. While it is generally thought that the drug forms intra-membrane pores through its preferential interaction with ergosterol in fungal cell membranes it is clear too that the drug can also form pores in cholesterol-containing mammalian cell membranes[12,13], which is why it can cause toxicity in patients. There is no direct *structural* evidence to support the idea of AmB-sterol pores, however, nor any structural characterization of the proposed complexes formed with sterols. In the studies reported here, the aim was to rectify this deficiency, employing neutron diffraction of oriented lipid-sterol multi-layers as a means to determine the structures of the AmB-perturbed lipid-sterol membranes and - more specifically - to determine the differences in the drug's interactions with synthetic human and fungal cell membranes, to help establish which (if any) of the various different models proposed for its interaction with membranes is correct[14–19].

Results

For each of the systems studied, the diffraction patterns show three orders of reflection, with sharp peaks (*cf*, Figure 1) indicating that the majority of their constituent bilayers are oriented parallel to the substrate surface. The structure factors for each of these systems, in each solvent contrast, are summarized in Table 1. The measured Bragg angles in each case were used in computing the *d*-spacings of the multilayers (*cf*, Supplementary Figure S1), and the phases of the structure factors readily obtained *via* linear correlation of the structure factor amplitudes and sample D_2O content (*cf*, Supplementary Figure S2).

The measured *d*-spacings for the POPC-ergosterol-AmB and POPC-cholesterol-AmB systems (Table 2) are the same as those estimated from small angle neutron scattering (SANS) studies of the equivalent lipid vesicles[20], and they are more or less the same for the two different systems (*viz.*, 55.5 Å *vs.* 56.8 Å, respectively). Their scattering length density profiles, however, are rather different from one another (Figure 2). For the ergosterol-containing system, there are minima in $\varphi(z)$ recorded at the bilayer center ($z = 0$ Å) and at $z = \pm 13$ Å, with

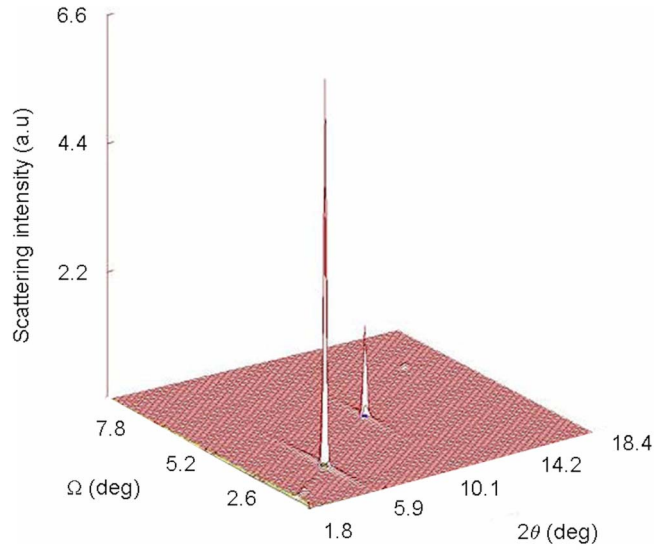

Figure 1 | Neutron diffraction pattern of the POPC-ergosterol bilayer stack recorded at 100% relative humidity in 100% D_2O and at ambient temperature; scattering intensity is plotted as a function of Ω (the angle between the incident beam and the sample plane – indicating the sample rotation) and 2θ (the angle between the incident and scattered beams).

intervening maxima at $z = \pm 6$ Å; for the cholesterol-containing system, there are minima found at the bilayer center and at $z = \pm 15.5$ Å, with intervening maxima at $z = \pm 9$ Å.

The scattering length density profiles for the unit cells for these two systems are modelled with the positions and widths of the distributions for their molecular components as shown in Table 2 and Figure 3. For the bilayers that incorporate AmB, regardless of whether they contain cholesterol or ergosterol, the slab thickness of the bilayers, d_B, is computed as around 44 Å (Table 3) – and these dimensions are consistent with the estimates obtained for the equivalent multilamellar systems which we previously determined by means of SANS studies of the AmB-containing lipid-sterol vesicles[20]. In the absence of AmB, the scattering length density profiles for the membranes (Supplementary Figure S3) are modelled with bilayer thicknesses of ~37 Å (Table 3), indicating that the insertion of drug into the bilayers leads to an increase in their thickness by ~7 Å.

In the POPC-cholesterol-AmB bilayers, the POPC molecules are found to be fairly extended - with an end-to-end length, L_{POPC}, of ~23 Å - and they show relatively little interdigitation (with a chain overlap of only ~ 1 Å) (Table 3). In the POPC-ergosterol-AmB bilayers, however, the POPC molecules are rather more extended - with an end-to-end length of ~26 Å - but the degree of interdigitation is also more pronounced, with a chain overlap of ~8 Å (Table 3). Inspection of the corresponding dimensions for the systems without AmB (see Table 3), show that these differences are due in large part to the differing influences of cholesterol and ergosterol on the POPC bilayers. Thus, even in the absence of AmB, the lipid chains are more extended in the bilayers containing ergosterol than those containing cholesterol (with L_{POPC} of 23 *vs.* 20 Å), and the chain overlap is also greater for the POPC-ergosterol bilayers (~9 Å *vs.* ~2 Å). These differences in the cholesterol *vs.* ergosterol-containing POPC bilayers are consistent with the differences in the lipid ordering for these systems determined through ^{2}H- and ^{13}C-NMR spectroscopic studies[21].

As regards the AmB and sterols incorporated in the POPC bilayers, there are two findings of particular significance, the first being that the distributions of the drug and sterol are *co-incident*, both for the ergosterol- and the cholesterol-containing systems, and

Table 1 | Structure factors for POPC-sterol and POPC-sterol-amphotericin multilayers

	% D_2O	$F_h(1)$	$F_h(2)$	$F_h(3)$
POPC-cholesterol	100	−12.38	12.77	−13.46
	75	−2.64	3.18	−10.44
	50	6.56	−5.19	−8.00
	0	19.56	−20.29	−0.5
POPC-ergosterol	100	−12.12	16.21	−5.76
	75	−1.47	4.93	−4.22
	50	4.05	−2.11	−3.48
	0	15.61	−15.11	0.00
POPC-cholesterol-AmB	100	−7.98	4.19	−3.85
	50	2.56	−1.17	−2.17
	0	13.56	−7.06	0.00
POPC-ergosterol-AmB	100	−8.52	5.13	−2.43
	75	−4.29	1.62	−1.88
	50	2.95	0.00	−2.04
	0	19.68	−5.78	0.00

Table 2 | Lamellar *d*-spacings and modelled bilayer component positions and distribution widths in POPC-sterol and POPC-sterol-amphotericin multilayers

	POPC-cholesterol		POPC-ergosterol	
	−AmB	+AmB	−AmB	+AmB
d-spacing	56.3	56.8	52.0	55.5
σ_{POPC}	8.0	9.2	9.5	10.5
z_{POPC}	± 8.5	± 10.6	± 7.0	± 9.0
σ_{Sterol}	± 7.0	5.0	± 7.0	6.0
z_{Sterol}	± 10.0	± 7.0	± 5.5	± 5.0
σ_{AmB}	-	5.0	-	6.0
z_{AmB}	-	± 7.0	-	± 5.0
ξ	20.0	20.4	18.0	19.0
z_S	± 2.5	± 3.3	± 3.2	± 3.9

Gaussian distribution half-widths, σ_i, for bilayer components *i*, centred at $z = \pm z_i$, and solvent distribution widths, ξ, centred at $z = \pm z_S$; all dimensions given in Å.

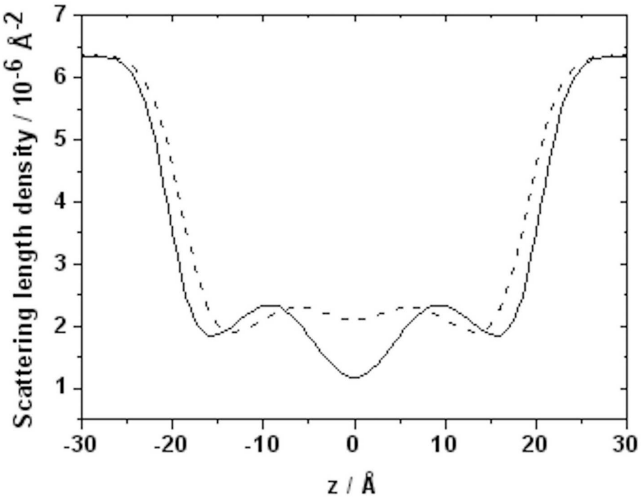

Figure 2 | Scattering length density profiles for POPC-sterol-AmB multilayers (cholesterol-containing system: solid line; ergosterol-containing system: dotted line). The scattering length density (in $Å^{-2}$) is plotted as a function of *z*, the distance along the normal to the bilayer (in Å), with the bilayer centre assigned as $z = 0$ Å.

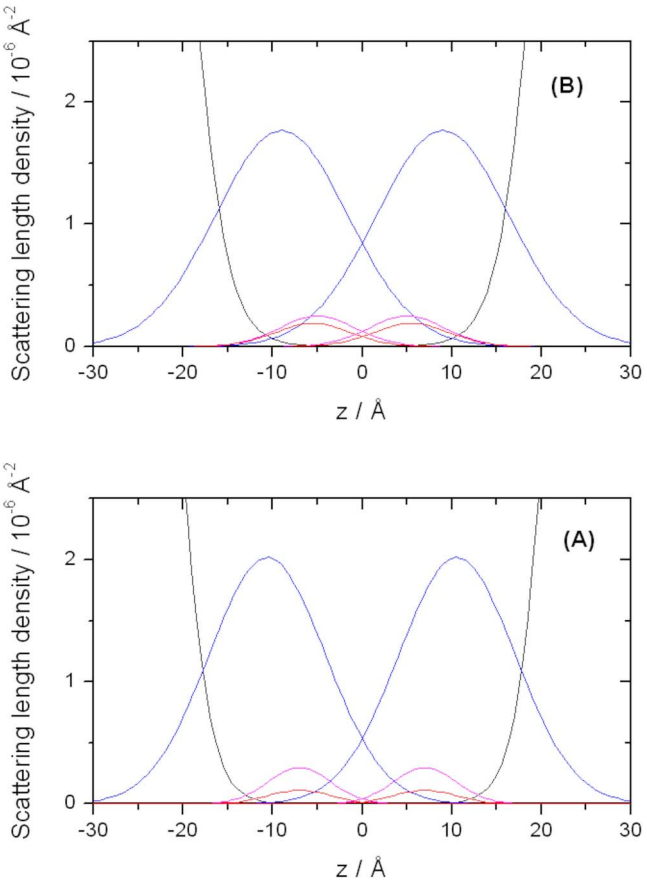

Figure 3 | Fitted scattering length density profiles for the bilayer constituents POPC (blue lines), cholesterol or ergosterol (red lines), AmB (magenta lines), and solvent (black lines). (A) POPC-cholesterol-AmB system; (B) POPC-ergosterol-AmB system. The scattering length density (in $Å^{-2}$) is plotted as a function of z, the distance along the normal to the bilayer (in Å), with the bilayer centre assigned as $z = 0$ Å. Note that for clarity in display of the AmB and sterol distributions, the scale on the ordinate is expanded, and so only the in-facing tails of the solvent *tanh* distributions are visible.

the second is that the AmB and sterol are found in *both* leaflets of the bilayers. In both the ergosterol- and cholesterol-containing bilayers, the centres of the AmB and water distributions are separated by 13-14 Å – indicating, therefore, that the AmB penetrates to more or less the same depth in the two types of bilayer.

When there is no AmB in the membranes, the cholesterol and ergosterol are about 17 Å end-to-end – which more or less matches their fully extended length – and when AmB is added, the molecules are seen to decrease in length, to around 12 Å in the case of cholesterol, and around 15 Å in the case of ergosterol (Table 3). The incorporation of AmB into the bilayers either leads, therefore, to the sterols becoming tilted with respect to the bilayer normal (by about 30° in the case of ergosterol and 45° in the case of cholesterol), or else to a change in their conformation, such that their side chains feature a higher proportion of *gauche* bonds.

Table 3 | Modelled bilayer dimensions and component lengths in POPC-sterol and POPC-sterol-amphotericin multilayers

	POPC-cholesterol		POPC-ergosterol	
	− AmB	+ AmB	− AmB	+ AmB
d_B	37	44	37	44
L_{POPC}	20	23	23	26
L_{Sterol}	17	12	17	15
L_{AmB}	-	12	-	15

Bilayer thickness, d_B, and end-to-end lengths, L_i, of bilayer components, i; all dimensions given in Å.

Discussion

Amphotericin (AmB) remains as our last line of defense against life-threatening systemic fungal infections, and although the recorded incidences of pathogen resistance to the drug are relatively rare at the present time, the frequency of resistance is muted to be rising[7–9]. That said, however, the usefulness of the drug – particularly in treatment of deep-seated fungal infections – is (and always has been) severely limited by its dose-dependent nephrotoxicity[10,11]. Efforts to improve the therapeutic index of the drug, or to develop related antimycotics with improved specificity, would thus benefit from a more complete understanding of the drug's mechanism of action.

Despite very extensive investigation over the past 40 years or so, however, the mechanism of action of AmB remains wholly unclear. The text book view is that AmB exerts its antifungal action by forming self-assembled ion channels (in complex with ergosterol) within fungal cell membranes, and that this subsequently leads to cell death through an indiscriminate transfer of ions across the membranes[12,13]. There is no direct structural evidence in support of this hypothesis, however, and recent research suggests that this accepted wisdom of the drug's mechanism of action may be altogether too simplistic.

The ability of AmB - and related polyene macrolides such as nystatin – to form self-assembled ion channels within cell membranes was established fairly early on, on the basis of ion and non-electrolyte permeability studies[12,13]. Models of these ion channels were subsequently proposed based purely on a consideration of the amphipathic structures of the drugs, together with an experimental demonstration of their co-operativity in development of the toxigenic membrane conductance[10]. The selective toxicity of AmB (and its related polyene macrolide antibiotics) towards ergosterol-containing fungal cell membranes compared to cholesterol-containing human cell membranes is thought to be a crucial factor in their specificity for fungi, with the commonly held view that the ion channels formed involve drug-sterol complexation, with ergosterol strongly preferred over cholesterol[13].

Recent studies, however, have shown that the macrolide antibiotic drugs' effects are influenced by their interactions with specific phospholipids[22], and that the manner of their interaction with cell membranes depends upon their concentration and aggregation state[18,23,24]. Linear dichroism FT-IR studies, moreover, seem to indicate that, in the presence of ergosterol, but *not* in the presence of cholesterol, a preponderance of AmB binds horizontally in the membrane, with the suggestion then that it may elicit its effects through a disruption of the lipid head groups, rather than by integrating (as oligomeric ion channels) into the bilayer[25]. Cotero and co-workers[16], and more recently, Venegas *et al.*[17] have shown that the role of sterols in AmB ion channel formation may be related to the effects they have on the structure of the membrane itself, rather than to a direct involvement in channel formation. Studies by Wang et *al.*[18] have suggested that the partitioning of polyene macrolide antibiotics into membranes may depend on the way in which the sterol is distributed within the plane of the membrane, showing a strong dependence on sterol concentration.

Even within the community of those who attribute AmB's mechanism of action to its complexation with sterols and the arrangement of these complexes as membrane pores, there is no clear consensus as to the nature and distribution of the pores that are formed (see Figure 4). Marty & Finkelstein proposed that there might be cation-selective "half-pores" which span just one leaflet of a bilayer (Figure 4C), and (co-existing) anion-selective aqueous channels (which comprise two aligned half-pores) that span the entire bilayer

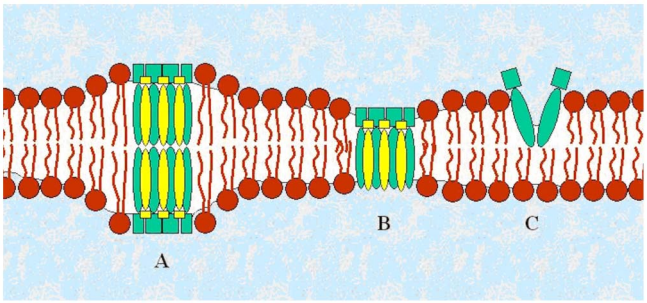

Figure 4 | Schematic illustration of the various different structures proposed for the pores formed by AmB in lipid bilayers: aligned half-pores/ion channels (A), half-width pores (B) and half-pores (C). AmB molecules shown in green, sterols, yellow, and phospholipids, red.

(Figure 4A)[14]. Evidence supporting such arrangements has recently been reviewed by Cohen[15]. Other researchers have proposed the idea of membrane spanning channels that are just one AmB molecule thick, inserted between the two bilayer leaflets, and giving rise to an associated membrane thinning (Figure 4B). Gray *et al.*, however, suggest that the antifungal action of AmB is primarily due to its sequesteration of ergosterol in the membrane, and that the formation of AmB-sterol pores constitutes a secondary, more minor component of its activity[19].

The diffraction data obtained here clearly indicate that the proposals made by Gagoś *et al.*[25] regarding the proportions of AmB that bind horizontally at the membrane surface *vs*. the proportions that insert vertically into the membrane are not correct. The data obtained for the POPC-ergosterol-AmB multilayers are consistent with a vertical insertion of AmB molecules into the bilayer – with the AmB spanning both leaflets – but with no evidence of any amount of AmB located at the bilayer surface (Gagoś *et al* suggesting that around 25% of the AmB binds in this manner for the POPC-ergosterol system). Likewise, for the POPC-cholesterol multilayers, whereas Gagoś *et al.* suggest that the proportions of horizontally-binding and vertically-inserting AmB are roughly 50 : 50, the data reported here suggest that the AmB only inserts vertically into the bilayer, with no evidence of either a change in scattering length density at the membrane surface nor of any increased *d*-spacing.

The studies reported here are also not consistent with the formation of single-length ion channels (as proposed by van Hoogevest & de Kruijff [r26]; Figure 4B) since such structures would give rise to a *decrease* in the mean bilayer thickness rather than the observed (4 Å) *increase*.

Our neutron diffraction derived AmB and sterol distributions are thus most plausibly modelled as double-length ion channels[14], similar to those shown in Figure 4A. It is also apparent from the neutron scattering length density profiles, however, that while the POPC-cholesterol-AmB bilayers have the cholesterol and AmB wholly contained within the separate leaflets of the bilayers, the POPC-ergosterol-AmB bilayers have both the AmB and ergosterol intruding from one leaflet into the opposing one. Such connectivity between the opposing half-pores within the ergosterol-containing bilayers could serve to stabilise the transmembrane ion-channels formed, and so account for the greater conductance of this system relative to that containing cholesterol, wherein the alignment of half-pores in opposing leaflets would vary with time and yield ion channels that were more ephemeral.

Sadly, our neutron diffraction profiles do not provide any substantive clue as to the nature of any interaction between AmB and cholesterol or ergosterol, and we are unable, therefore, to determine whether the drug and sterols are arranged head-to-head or head-to-tail[27,28]. It is interesting to note, however, that when the AmB inserts into the POPC-ergosterol membrane, it is either more extended or less tilted than when it inserts into the POPC-cholesterol membrane, and this might easily be accounted for by its mycosamine head group adopting different orientations in the two systems (which Matsumori and co-workers suggest as a primary determinant of the drug's antifungal activity[29]). Taken together with our observation that the insertion of the drug causes only a 0.5 Å perturbation in the location of ergosterol in the membrane but causes a 3 Å shift in the position of cholesterol (Table 2), it is clear that there may be entropic as well as enthalpic contributions to account for the drug's preferred interaction with ergosterol-containing membranes (this in turn accounting for the drug's selectivity for fungal cell membranes).

Methods

Sample preparation. All solvents, together with cholesterol, ergosterol and amphotericin B (AmB) were purchased from Sigma Aldrich Co. Ltd. (Dorset, UK). d_{31}-1-palmitoyl-2-oleoyl-*sn*-glycero-3-phosphocholine (d_{31}-POPC) was purchased from Avanti Polar Lipids Inc. (Alabama, USA). All chemcials were used as received.

The oriented lipid multi-layer samples were prepared using (70 : 30 mol%) POPC-sterol mixtures dispersed in chloroform:methanol (2 : 1 v/v, 5 mL, spectroscopic grade) at a concentration of ~10 mg mL^{-1}, in the absence and presence of 5 mol% AmB.

All samples were prepared using d_{31}-POPC, and *h*-sterols and *h*-AmB. The lipid (/sterol) dispersions were deposited onto a Si(100) substrate with native oxide (Si-Mat, Landsberg/Lech, Germany – surface area of 19.6 cm^2) previously cleaned by successive ultrasonications in acetone, ethanol and methanol followed by a final UV-O_3 treatment for about 30 min[28].

900 µL of sample were deposited onto the wafer in order to coat the support with ~1000 bilayers (this volume calculated on the basis of the area of the silicon wafer). The deposition was made by means of the "rock and roll" method[29,30]. In order to remove all residual organic solvent from the samples, the wafers were stored under vacuum overnight. Samples were then annealed and hydrated using the required mixture of D_2O and H_2O, maintaining the samples in a dessicator containing a saturated solution of sodium sulphate in the required solvent mixture, in an oven at 50°C for at least 24 hours.

Neutron diffraction. In order to establish the location of AmB within the model fungal and mammalian cell membranes, neutron diffraction patterns were recorded for 70 : 30 mol% POPC-ergosterol and POPC-cholesterol oriented multilayers in the presence and absence of (5 mol%) AmB. The entire set of experiments was performed with samples maintained at 100% relative humidity – in order to approximate the situation *in vivo* – with each prepared and measured under four different H/D contrasts achieved using D_2O/H_2O mixtures involving 100% D_2O; 75% D_2O; 50% D_2O and 100% H_2O.

Experiments were performed on the D16 diffractometer at the Institute Laue-Langevin (ILL, Grenoble, France) operating with neutrons of wavelength (λ) of 4.75 Å, in the reflection mode. Samples were mounted on a goniometer held in a sealed temperature-controlled aluminum humidity chamber in the presence of a saturated sodium sulphate to maintain constant maximum humidity. The temperature of the sample chamber was maintained at 25°C. The sample-to-detector distance was set at 1.0 m, and the intensity of the diffracted neutron beam recorded using a position-sensitive two-dimensional ^{3}He detector with 128×128 channels and 2 mm resolution between channels. The two-dimensional detector readout was integrated in the vertical direction, giving a one-dimensional intensity projection as a function of the detector channel position (2θ). Intensities on the detector surface were corrected by normalization to a water calibration and by subtraction of the empty chamber background.

The lamellar repeat distance (*d*-spacing, *d* Å) for each of the diffracting samples was computed as $1/2s$ where *s* is the slope calculated for the linear regression of $sin\theta$ on $h\lambda$., where θ is the angle of diffraction for the h^{th} order diffraction peak (Supplementary Fig. S1). The positions and scattering intensities of the diffraction peaks were computed with peak fitting and integration using the ILL in-house LAMP software.

Data analysis. The corrected intensities of the diffraction peaks ($I_{cor}(h)$), were obtained from the observed intensities ($I_{obs}(h)$) as:

$$I_{cor}(h) = I_{obs}(h)\frac{\sin 2\theta}{A_h(h)B(h)}$$

where $B(h)$ is the acceptance correction (here taken as 1.0)[31] and $A_h(h)$ is the correction factor for sample adsorption[31,32]:

$$A_h(h) = \frac{\sin\theta}{2\mu T}\cdot\left(1 - e^{\frac{-2\mu T}{\sin\theta}}\right)$$

$A_h(h)$ is dependent upon the diffraction angle (θ), the sample thickness (T), and the linear attenuation coefficient (μ) - which is calculated from the wavelength of the incident neutrons, and the sample composition and density[33].

The amplitudes of the structure factors for the diffracting sample, $|F_h(h)|$, were obtained[34,35] from the corrected Bragg peak intensities as:

$$|F_h(h)| = \sqrt{I_{cor}(h) \cdot h}$$

the multiplier, h, here approximating the Lorentz correction factor[34].

The unit cells of the diffracting samples were assumed to be centrosymmetric (that is, with centres of symmetry at $z = 0$ and $z = \pm d/2$, where d is the d-spacing of the multilayers) and so their scattering length density profiles ($\varphi(z)$) in the direction normal to the sample surface (z) were obtained by the Fourier summation[34]:

$$\varphi(z) = \frac{2}{d} \cdot \sum_{h-1}^{h} |F_h(h)| \cdot \varepsilon(h) \cdot \cos\left(2\pi \frac{hz}{d}\right)$$

where the signs of the structure factors ($\varepsilon(h)$) take values of + 1 or –1. The signs of the different structure factors were determined from plots of $|F_h(h)|$ *vs.* % D_2O[36], and arranging that the plotted points fall on a straight line (Supplementary Fig. S2)[37,38]. The expected signs of the slopes of these plots were determined as positive, according to the method reported by Léonard *et al.*[38], assuming water distribution width (d_w) to d-spacing (d) ratios of physically sensible magnitudes (*viz.*, $0.05 \leq d_w/d \leq 0.25$). The phases for the structure factors with h odd were then reversed in order to shift the unit cell origin from the centre of the water distribution to the centre of the bilayer[38].

Bilayer structure modelling. Modelling of the scattering length density profiles for the samples was performed by refining the relative position of each bilayer constituent (i), given its neutron scattering length, b_i, and its molecular interfacial area, a_0. The POPC, sterol, and amphotericin within the bilayer were each modelled by means of Gaussian distributions, with the variation in scattering length density for the individual components, $\rho_i(z)$ computed as:

$$\rho_i(z) = \left(\frac{1}{a_0 \pi^{\frac{1}{2}}}\right) \cdot \frac{b_i}{\sigma_i} \cdot \exp\left(\frac{z - z_i}{\sigma_i}\right)^2$$

with the Gaussian centred at z_i, with half width, σ_i. The interfacial areas per molecule of each component were taken as 72 Å^2 for POPC, 39 Å^2 for cholesterol and ergosterol, and 29 Å^2 for AmB. The scattering length density profile for the solvent in the multi-layer was modelled assuming a *tanh* distribution at each end of the unit cell:

$$\rho_s(z) = \rho_{D_2O} \cdot \left\{\frac{1}{2} + \frac{1}{2}\tanh\frac{z - z_S}{\xi}\right\}$$

with the distributions having width, ξ, and centred at $\pm z_S$.

The end-to-end lengths of the bilayer components, i, were computed from the modelled Gaussian distribution half-widths (σ_i) as:

$$L_i = \sqrt{\frac{12}{8}} \cdot (2 \cdot \sigma_i)$$

and the bilayer slab thicknesses, d_B, then obtained as:

$$d_B = L_{POPC} + 2 \cdot |Z_{POPC}|$$

where $2.|z_{POPC}|$ is the separation between the mid-points of the POPC distributions in the two leaflets of the bilayer. The interdigitation of the POPC chains was hence obtained as:

$$ID = L_{POPC} - 2 \cdot |Z_{POPC}|$$

1. Enoch, D. A., Ludlam, H. A. & Brown, N. M. Invasive fungal infections: a review of epidemiology and management options. *J Med. Microbiol.* **55**, 809–818 (2006).
2. Warnock, D. W. Trends in the epidemiology of invasive fungal infections. *J. Med. Mycol.* **48**, 809–818 (2007).
3. Lass-Flo, C. The changing face of epidemiology of invasive fungal disease in Europe. *Mycoses* **52**, 197–205 (2009).
4. White, T. C., Marr, K. A. & Bowden, R. A. Clinical, cellular, and molecular factors that contribute to antifungal drug resistance. *Clinical Microbiol. Rev.* **11**, 382–402 (1998).
5. Vandeputte, P., Ferrari, S. & Coste, A. T. Antifungal resistance and new strategies to control fungal infections. *Int. J. Microbiol.* **2012**, Article ID 713687 (2012).
6. Pfaller, M. A. Antifungal drug resistance: mechanisms, epidemiology, and consequences for treatment. *Am. J. Med.* **125** (Suppl 1), S3–S13 (2012).
7. Shin, J. H. *et al.* Detection of amphotericin B resistance in *Candida haemulonii* and closely related species by use of the Etest, Vitek-2 yeast susceptibility system, and CLSI and EUCAST broth microdilution methods. *J Clinical Microbiol.* **50**, 1852–5 (2012).
8. Sutton, D. A. *et al.* In vitro amphotericin B resistance in clinical isolates of *Aspergillus terreus*, with a head-to-head comparison to voriconazole. *J. Clinical Microbiol.* **37**, 2343–2345 (1999).
9. Hadrich, I. *et al.* Amphotericin B resistance is associated with fatal *Aspergillus flavus* infection. *Medical Mycology* **2012**, EPUB 1–6 (2012).
10. Gallis, H. A., Drew, R. H. & Pickard, W. W. Amphotericin B: 30 years of clinical experience. *Rev. Infect. Diseases* **12**, 308–329.
11. Deray, G. Amphotericin B nephrotoxicity. *J. Antimicr. Chemother.* **49** (Suppl. S1) , 37–41 (2002).
12. Finkelstein, A. & Holz, R. Aqueous pores created in thin lipid membranes by the polyene antibiotics nystatin and amphotericin B. *Membranes* **2**, 377–348 (1973).
13. Hsuchen, C.-C. & Feingold, D. S. Selective membrane toxicity of the polyene antibiotics: studies on lecithin model membranes (liposomes). *Antimicrob. Agents Chemother.* **4**, 309–315 (1973).
14. Marty, A. & Finkelstein, A. Pores formed by nystatin. differences in its one-side and two-side action. *J. Gen. Physiol.* **65**, 515–526 (1975).
15. Cohen, B. E. A sequential mechanism for the formation of aqueous channels by amphotericin-B in liposomes – the effect of sterols and phospholipid-composition, *Biochim. Biophys. Acta - Biomembranes* **1108**, 49–58 (1992).
16. Cotero, B. V., Rebolledo-Antunez, S. & Ortega-Blake, I. On the role of sterol in the formation of the amphotericin B channel. *Biochim. Biophys. Acta - Biomembranes* **1375**, 43–51 (1998).
17. Venegas, B., González-Damián, J., Celis, H. & Ortega-Blake, I. Amphotericin B channels in the bacterial membrane: role of sterol and temperature. *Biophys. J.* **85**, 2323–2332 (2003).
18. Wang, M. M., Sugar, I. P. & Chong, P. L. G. Role of the sterol superlattice in the partitioning of the antifungal drug nystatin into lipid membranes. *Biochem.* **37**, 11797–11805 (1998).
19. Gray, K. C. *et al.* Amphotericin primarily kills yeast by simply binding ergosterol. *Proc. Natl. Acad. Sci. (U.S.A)* **109**, 2234–2239 (2012).
20. Foglia, F. F. *et al.* Small angle neutron scattering studies of the effects of amphotericin B on phospholipid and phospholipid-sterol membrane structure. *Biochim. Biophys. Acta - Biomembranes* **1808**, 1574–1580 (2010).
21. Urbina, J. A. *et al.* Molecular order and dynamics of phosphatidylcholine bilayer membranes in the presence of cholesterol, ergosterol and lanosterol: a comparitive study using ^{2}H, ^{13}C and ^{31}P-NMR spectroscopy. *Biochim. Biophys. Acta – Biomembranes* **1238**, 163–176 (1995).
22. Katarzyna, H. W. & Patrycja, D. L. Interaction between nystatin and natural membrane lipids in Langmuir monolayers - The role of a phospholipid in the mechanism of polyenes' mode of action. *Biophys. Chem.* **123**, 154–161 (2006).
23. Minones, J., Conde, O., Dynarowicz-Latka, P. & Casas, M. Penetration of amphotericin B into DOPC monolayers containing sterols of cellular membranes. *Colloids & Surfaces A* **270**, 129–137 (2005).
24. Herec, M., Islamov, A., Kuklin, A., Gagoś, M. & Gruszecki, W. I. Effect of antibiotic amphotericin B on structural and dynamic properties of lipid membranes formed with egg yolk phosphatidylcholine. *Chem. Phys. Lipids* **147**, 78–86 (2007).
25. Gagoś, M., Gabrielska, J., Dalla Serra, M. & Gruszecki, W. I. Binding of antibiotic amphotericin B to lipid membranes: monomolecular layer technique and linear dichroism-FTIR studies. *Mol. Membrane Biol.* **22**, 433–442 (2005).
26. van Hoogevest, P. & de Kruijff, B. Effect of amphotericin on cholesterol-containing liposomes of egg phosphatidylcholine and didocosenoyl phosphatidylcholine. *Biochim. Biophys. Acat – Biomembranes* **511**, 397–407 (1978).
27. Matsumori, N., Sawada, Y. & Murata, M. Mycosamine Orientation of amphotericin B controlling interaction with ergosterol: sterol-dependent activity of conformation-restricted derivatives with an amino-carbonyl bridge. *J. Am. Chem. Soc.* **127**, 10667–10675 (2005).
28. Schneck, E. *et al.* Mechanical properties of interacting lipopolysaccharide membranes from bacteria mutants studied by specular and off-specular neutron scattering. *Phys. Rev. E* **80**, 041929/1 (2009).
29. Tristram-Nagle, S. *et al. Biophys. J.* **64**, 1097–??? (1993).
30. Tristram-Nagle, S., Liu, Y., Legleiter, J. & Nagle, J. F. Structure of gel pahse DMPC determined by X-ray diffraction. *Biophys. J.* **83**, 3324–3335 (2002).
31. Franks, N. P. & Lieb, W. R. Structures of lipid bilayers and the effects of general anaesthetics: X-ray and neutron diffraction study. *J. Mol. Biol.* **133**, 469–500 (1979).
32. Han, X. & Hirstova, K. Viewing the bilayer hydrophobic core using neutron diffraction. *J. Membrane Biol.* **227**, 123–131 (2009).
33. www.ncnr.nist.gov/instruments/bt1/neutron.html
34. Gogol, E. P., Engelman, D. M. & Zaccai, G. Neutron diffraction analysis of cytochrom b5 reconstituted in deuterated lipid bilayers. *Biophys. J.* **43**, 285–292 (1983).
35. Zaccai, G., Blasie, J. K. & Schoenborn, B. P. Neutron diffraction studies on location of water in lecithin bilayer model membranes. *Proc. Natl. Acad. Sci. (USA)* **72**, 376–380 (1975).
36. Jacobs, R. E. & White, S. H. The nature of the hydrophobic binding of small peptides at the bilayer interface – implications for the insertion of transbilayer helices. *Biochem.* **28**, 3421–3437 (1989).
37. Worcester, D. L. & Frank, N. P. Structural analysis of hydrated egg lecithin and cholesterol bilayers 2. Neutron diffraction. *J. Mol. Biol.* **100**, 359–378 (1976).
38. Léonard, A. *et al.* Location of cholesterol in DMPC membranes: a comparative study by neutron diffraction and molecular mechanics simulation. *Langmuir* **17**, 2019–2030 (2001).

Acknowledgements

FF was supported by EPSRC grant EP/F021291/1. The authors thank the Institut Laue-Langevin (Grenoble, France) for use of the D16 diffractometer.

Author contributions

MJL and DJB conceived the study. FF and DJB performed the measurements, with advice and assistance in sample preparation from GF, and instrument set-up, calibrations and

operating instruction provided by BD. DJB analysed the data, and prepared the manuscript with contributions provided by FF and MJL.

Additional information

Supplementary information accompanies this paper at http://www.nature.com/scientificreports

Competing financial interests: The authors declare no competing financial interests.

How to cite this article: Foglia, F., Lawrence, M.J., Demé, B., Fragneto, G. & Barlow, D. Neutron diffraction studies of the interaction between amphotericin B and lipid-sterol model membranes. *Sci. Rep.* **2**, 778; DOI:10.1038/srep00778 (2012).